Amphibolites with staurolite and other aluminous minerals: calculated mineral equilibria in NCFMASH

J. ARNOLD,[1] R. POWELL[2] AND M. SANDIFORD[3]
[1]*Department of Earth Sciences, The University of Queensland, Qld 4072, Australia (email: jarnold@earthsciences.uq.edu.au),* [2]*School of Earth Sciences, The University of Melbourne, Parkville, Vic 3052, Australia,* [3]*Department of Geology and Geophysics, The University of Adelaide, SA 5005, Australia*

ABSTRACT Amphibolite facies mafic rocks that consist mainly of hornblende, plagioclase and quartz may also contain combinations of chlorite, garnet, epidote, and, more unusually, staurolite, kyanite, sillimanite, cordierite and orthoamphiboles. Such assemblages can provide tighter constraints on the pressure and temperature evolution of metamorphic terranes than is usually possible from metabasites. Because of the high variance of most of the assemblages, the phase relationships in amphibolites depend on rock composition, in addition to pressure, temperature and fluid composition. The mineral equilibria in the Na_2O–CaO–FeO–MgO–Al_2O_3–SiO_2–H_2O (NCFMASH) model system demonstrate that aluminium content is critical in controlling the occurrence of assemblages involving hornblende with aluminous minerals such as sillimanite, kyanite, staurolite and cordierite. Except in aluminous compositions, these assemblages are restricted to higher pressures. The iron to magnesium ratio (X_{Fe}), and to a lesser extent, sodium to calcium ratio, have important roles in determining which (if any) of the aluminous minerals occur under particular pressure–temperature conditions. Where aluminous minerals occur in amphibolites, the P–T–X dependence of their phase relationships is remarkably similar to that in metapelitic rocks. The mineral assemblages of Fe-rich amphibolites are typically dominated by garnet- and staurolite-bearing assemblages, whereas their more Mg-rich counterparts contain chlorite and cordierite. Assemblages involving staurolite–hornblende can occur over a wide range of pressures (4–10 kbar) at temperatures of 560–650 °C; however, except in the more aluminous, iron-rich compositions, they occupy a narrow pressure–temperature window. Thus, although their occurrence in 'typical' amphibolites may be indicative of relatively high pressure metamorphism, in more aluminous compositions their interpretation is less straightforward.

Key words: petrogenetic grid; phase diagram; P–T pseudosections; THERMOCALC; T–X pseudosections.

INTRODUCTION

Metamorphosed mafic rocks in orogenic belts usually involve high-variance assemblages which are stable over very large regions of pressure (P)–temperature (T) and compositional (X) space. In particular, amphibolite facies mafic rocks typically contain the 'common' assemblage: hornblende, plagioclase, epidote, chlorite ± garnet (Laird, 1980). As a consequence of this apparent simplicity, it has proved difficult to extract precise P–T constraints from amphibolite assemblages. However, aluminous minerals such as staurolite, kyanite, sillimanite, cordierite and orthoamphiboles also occur with hornblende, plagioclase and quartz in some mafic rocks. Because of their lower variance and the common development of reaction textures, these assemblages have great potential for constraining equilibration conditions, reaction history and P–T evolution. Calculated mineral equilibria focusing on these assemblages should improve our understanding of the phase relationships of mafic rocks as a function of pressure, temperature and bulk rock composition.

Aluminous minerals found in association with hornblende, plagioclase and quartz in amphibolites include epidote, chlorite, garnet, kyanite, sillimanite, staurolite, cordierite and gedrite (i.e. aluminous orthoamphibole). Whereas the presence of epidote, chlorite and/or garnet is commonplace in mafic rocks, the other aluminous minerals are rare, although widely distributed (e.g. Spear, 1982; Selverstone *et al*., 1984; Arnold *et al*., 1995). A summary of documented occurrences of amphibolites bearing aluminous minerals is given in Table 1. Of primary interest is the question of how amphibolites containing aluminous minerals are related to the common assemblage (e.g. Helms *et al*., 1987). This question will be addressed below using P–T and T–X pseudosections. The assemblages could be related in the following two obvious ways:

1 Amphibolites containing aluminous minerals, such as staurolite and kyanite, have similar bulk compositions to those that develop the common assemblage, but equilibrate at different P–T conditions (Selverstone *et al*., 1984; Helms *et al*., 1987).

2 Amphibolites containing aluminous minerals, such as staurolite and kyanite, have different bulk compositions from those that develop the common assemblage, but equilibrate at similar P–T conditions (Spear, 1982;

Table 1. Reported low-variance assemblages of kyanite, staurolite and other aluminous minerals with hornblende (all + Pl + Qtz + H_2O).

NCFMASH invariant/univariant	Label of sub-assemblage	Assemblage[1]	References
[Crd,Oam]		Ky St Grt Chl Ep Hbl	Selverstone *et al.* (1984)
[Crd,Oam,Czo]		As St Grt Chl Hbl	
	[As,Crd,Chl,Oam,Czo]	St Grt Hbl	Frey (1980); Ward (1984); Grew & Sandiford, 1985; Arnold (1994)
	[As,Crd,Grt,Oam,Czo]	St Chl Hbl	Humphreys (1993)
	[As,Crd,Oam,Czo]	St Grt Chl Hbl	Spear (1982); Selverstone *et al.* (1984); Helms *et al.* (1987)
	[Crd,Chl,Oam,Czo]	Ky St Grt Hbl	Gibson (1978); Frey (1980); Selverstone *et al.*, 1984
	[Crd,Grt,Chl,Oam,Czo]	Ky St Hbl	Gibson (1978); Frey (1980); Selverstone *et al.*, 1984; Arnold (1994)
	[Crd,Grt,Chl,Oam,Czo]	Sil St Hbl	Humphreys (1993)
	[Crd,Grt,Oam,Czo]	Ky St Chl Hbl	Humphreys (1993)
	[St,Crd,Chl,Oam,Czo]	Ky Grt Hbl	Frey (1980)
	[St,Crd,Grt,Oam,Czo]	Ky Chl Hbl	Helms *et al.*, 1987
	[St,Crd,Grt,Oam,Czo]	Sil Chl Hbl	Humphreys (1993)
[St,Crd,Oam]		As Grt Chl Czo Hbl	
	[As,St,Crd,Chl,Oam]	Grt Ep Hbl 2Pl	Spear (1982)
	[As,St,Crd,Oam]	Grt Chl Ep Hbl	Selverstone *et al.* (1984)
	[As,St,Crd,Oam,Czo]	Grt Chl Hbl	Selverstone *et al.* (1984)
	[St,Crd,Oam,Czo,Hbl]	Ky Grt Chl	Humphreys (1993)
	[St,Crd,Grt,Oam]	Ky Chl Ep Hbl	Selverstone *et al.* (1984)
[Crd,Grt,Oam]		Ky St Chl Ep Hbl	Selverstone *et al.* (1984)
	[As,Crd,Grt,Chl,Oam,Czo]?	St Hbl?	Whitney (1992)
	[As,Crd,Grt,Chl,Oam]	St Czo Hbl	Ward (1984)
[Crd,Chl,Oam]		Ky St Grt Czo Hbl	Purtscheller & Mogessie (1984)
[As,Crd,Oam]		St Grt Chl Ep Hbl	Selverstone *et al.* (1984)
[Crd,Czo]		As St Grt Chl Oam Hbl	
[Crd,Chl,Czo]		As St Grt Oam Hbl	
	[As,Crd,Chl,Czo]	St Grt Ged Hbl	Spear (1982); Arnold (1994)
	[As,Crd,Grt,Chl,Czo]	St Ged Hbl	Humphreys (1993)
	[Crd,Grt,Chl,Czo]	Ky St Ged Hbl	Ward (1984); Arnold (1994)
	[Crd,Grt,Chl,Czo]	Sil St Ged Hbl	Schumacher & Robinson (1987)
[Crd,Grt,Czo]		Ky St Chl Ged Hbl	Ward (1984); Helms *et al.* (1987)
	[As,Crd,Grt,Czo]	St Chl Ged Hbl	Spear (1982)
[As,Crd,Czo]		St Grt Chl Ged Hbl	Spear (1982)
	[As,St,Crd,Czo]	Grt Chl Ged Hbl	Spear (1982); Helms *et al.* (1987)
[Grt,Chl,Czo]		Sil St Crd Ged Hbl	Schumacher & Robinson (1987)
	[As,Grt,Chl,Czo]	St Crd Ged Hbl	Schumacher & Robinson (1987)
	[Grt,Chl,Oam,Czo]	Sil St Crd Hbl	Humphreys (1993)
[St,Grt,Czo]		As Crd Chl Oam Hbl	
	[St,Grt,Chl,Czo]	Ky Crd Ath Hbl	Arnold (1994)
	[St,Grt,Chl,Czo]	Sil Crd Ath Hbl	Schumacher & Robinson (1987)
[St,Chl,Czo]		As Crd Grt Oam Hbl	
	[St,Crd,Chl,Oam,Czo]	Ky Grt Hbl	See above
	[St,Grt,Chl,Czo]	Ky Crd Ath Hbl	See above
	[St,Grt,Chl,Czo]	Sil Crd Ath Hbl	See above
	[As,St,Chl,Czo]	Crd Grt Ged Hbl	Humphreys (1993)

[1] Note that many assemblages are related to two or more univariants; each is listed once only. For abbreviations see Table 2.

Purtscheller & Mogessie, 1984; Selverstone *et al.*, 1984; Ward, 1984; Grew & Sandiford, 1985).

Although these hypotheses appear to be easily distinguishable, this is not necessarily so. For example, even if staurolite-bearing amphibolites can occur in bulk compositions similar to the common assemblage over a narrow range of *P–T*, this range of *P–T* may expand for more aluminous bulk compositions. Furthermore, identifying the range of bulk compositions in which the common assemblage can be developed is difficult, particularly as this range is a function of *P–T*. This difficulty arises primarily because of the wide compositional ranges of the minerals involved. Thus, when correlating the analysed compositions of rocks with their mineral assemblages, identifying the compositional differences that may give rise to mineralogical differences presents a formidable problem.

We approach this problem by examining an 'average' amphibolite, which could be expected to develop the common assemblage, and then considering bulk compositions flanking this average. The average amphibolite we use is an average of 20 bulk rock analyses of greenstones and amphibolites from Vermont, which occur as dykes or volcanics of dominantly tholeiitic affinity (bulk composition A (Laird; 1980); Table 2). This bulk composition is intermediate to those presented by Cady (1969), Cooper & Lovering (1970), Helms *et al.* (1987) and Yardley (1989), and thus provides an appropriate composition to address the role of bulk composition and *P–T* in the development of mineral assemblages in amphibolites.

This paper, and particularly the phase diagrams herein, document how phase relationships respond to compositional variation from this 'average' amphibolite. For simplicity, the compositional vectors employed are simple and do not attempt to mimic the chemical changes that may result from particular petrological processes. This is appropriate in view of the compositional spread of 'amphibolites' and the range of

Table 2. Bulk compositions for *P–T* pseudosections.

Label	Fig.	Al_2O_3[1]	CaO	MgO	FeO	Na_2O	X_{Fe}
A	4	22.23	28.10	29.03	14.83	5.81	0.338
A + 2 Pl[2]	6	24.23	32.10	29.03	14.83	3.81	0.338
A - 2 Pl	6	20.23	24.10	29.03	14.83	7.81	0.338
A (Al_{10})	7	10	32.51	33.6	17.165	6.725	0.338
A (Al_{50})	7	50	18.06	18.665	9.535	3.74	0.338
B	8	34	23.84	24.64	12.59	4.93	0.338
B (X_{Fe} 0.5)	11	34	23.84	18.615	18.615	4.93	0.5
C	13	26	26.73	27.63	14.11	5.53	0.338
C (X_{Fe} 0.5)	15	26	26.73	20.87	20.87	5.53	0.5

[1] THERMOCALC uses moles of cations, written in terms of oxides. [2]2 Pl signifies variation by two units of plagioclase substitution, 2 ($Ca_{-1}Al_{-1}Na_1Si_1$).

mechanisms through which chemical changes can be achieved. We address the dependence of the phase relationships in amphibolites on *P*, *T* and bulk composition using the software THERMOCALC (Powell & Holland, 1988; Powell *et al*., 1998). THERMOCALC version 2.6 (Powell *et al*., 1998) is used with the internally consistent thermodynamic dataset of 11 December 1996 (Holland & Powell, 1990). The program allows the phase compositions to be calculated along the reactions, marking a major departure from the use of fixed composition phases (e.g. Spear & Rumble, 1986). Recently incorporated facilities in THERMOCALC allow direct calculation of boundary lines and points on fields of any variance in *P–T* and *T–X* pseudosections (Powell *et al*., 1998), and have made possible the consideration of the dominantly high-variance equilibria in this study.

THE MODEL SYSTEM Na_2O–CaO–FeO–MgO–Al_2O_3–SiO_2–H_2O

The minerals of interest in this study include those of Laird's common assemblage (Laird, 1980): hornblende, plagioclase, epidote (or clinozoisite), chlorite, garnet and quartz, as well as aluminous minerals more commonly associated with metapelitic rocks. Other minerals reported in equilibrium with hornblende are sillimanite, kyanite, staurolite, cordierite, garnet, anthophyllite, gedrite, biotite or phlogopite, muscovite, phengite or paragonite, calcite, ankerite or dolomite, and, more rarely, spinel, corundum, sapphirine and andalusite. Minor minerals include titanite, ilmenite, rutile, magnetite, ülvospinel, pyrite, pyrrhotite, apatite, monazite and allanite (see references in Table 1). The major minerals can be described within the system Na_2O–K_2O–CaO–FeO–MgO–Fe_2O_3–MnO–TiO_2–Al_2O_3–SiO_2–H_2O–CO_2, whereas many of the minor minerals are stabilized by small amounts of phosphorus, sulphur and rare-earth elements that are not important in the major minerals. Of the 12 main components, CO_2, K_2O and TiO_2 are commonly restricted to only one mineral, e.g. calcite, dolomite or ankerite, biotite, muscovite or paragonite, ilmenite, rutile or titanite. As such, it is valid to assume that CO_2, K_2O and TiO_2 have little effect on the relationships among the remaining minerals and thus may be neglected (or 'projected from'). Amphibolites with more than one carbonate-, K- or Ti-bearing mineral are outside the scope of these calculations. MnO tends to be restricted to garnet in amphibolites and can expand the stability field for garnet (e.g. Mahar *et al*., 1997). However, because observed Mn contents are generally low, it is excluded from the model system. Fe_2O_3 is important in a number of minerals in amphibolites, especially epidote, but also in hornblende, as well as several opaque minerals. However, thermodynamic data for ferric iron-bearing mineral end-members, apart from epidote, are not yet available. So, of necessity, Fe_2O_3 is also omitted from the analysis. These phase diagrams may be thought of as 'projections' from epidote. All of the remaining components, Na_2O–CaO–FeO–MgO–Al_2O_3–SiO_2–H_2O (NCFMASH), are important in reflecting the main substitutions in the principal minerals of amphibolites. The phases of interest, end-member compositions and abbreviations are listed in Table 3. In this model system, Laird's common assemblage (Laird, 1980) involves hornblende, plagioclase, clinozoisite, chlorite, garnet and quartz.

In order to focus attention on the changes in 'equilibrium' assemblages with changes in *P*, *T* and *X*, the effective size of the multi-component system can be reduced by considering minerals that are always present to be 'in excess'. For example, in the model metapelite system K_2O–FeO–MgO–Al_2O_3–SiO_2–H_2O (KFMASH), muscovite, quartz and H_2O are usually taken to be in excess (at least below the mid-amphibolite facies), so that phase relationships can be illustrated in a two-dimensional compatibility diagram (AFM: Thompson, 1957). NCFMASH can be reduced to an effective quaternary by considering plagioclase, quartz and aqueous fluid to be in excess (e.g. Spear, 1982). This depiction has the advantage of showing explicitly the bulk compositions and assemblages that do and do not contain hornblende (Fig. 1); however the plotting positions and tie lines in three dimensions are extremely difficult to read (e.g. fig. 12 in Spear, 1982). NCFMASH can be further reduced to an effective ternary by also taking hornblende to be in excess. Such an assumption means that assemblages lacking any one of these minerals cannot be considered, and thus that the rare quartz-absent assemblages of hornblende with corundum, sapphirine or spinel cannot be dealt with here. In practice, this does not unduly

Table 3. Mineral abbreviations and formulae.

Mineral/end-member name	Abbreviation (general)	Abbreviation (THERMOCALC)	Formula
Aluminosilicates	As		
Andalusite	And	*and*	Al_2SiO_5
Sillimanite	Sil	*sill*	Al_2SiO_5
Kyanite	Ky	*ky*	Al_2SiO_5
Staurolite	St[1]	*st*	
Fe-staurolite		*fst*	$Fe_4Al_{18}Si_{7.5}O_{44}(OH)_4$
Mg-staurolite		*mst*	$Mg_4Al_{18}Si_{7.5}O_{44}(OH)_4$
Zn-staurolite		*znst*	$Zn_4Al_{18}Si_{7.5}O_{44}(OH)_4$
Chlorite	Chl[2]	*chl*	
Clinochlore		*clin*	$Mg_4(MgAl)Si_2[AlSi]O_{10}(OH)_8$
Daphnite		*daph*	$Fe_4(MgAl)Si_2[AlSi]O_{10}(OH)_8$
Amesite		*ames*	$Mg_4(Al_2)Si_2[Al_2]O_{10}(OH)_8$
		spch	$Mg_6Si_4O_{10}(OH)_8$
Cordierite	Crd	*cd*	
Mg-cordierite		*crd*	$Mg_2Al_4Si_5O_{18}$
Fe-cordierite		*fcrd*	$Fe_2Al_4Si_5O_{18}$
Hydrous cordierite		*hcrd*	$Mg_2Al_4Si_5O_{18}.H_2O$
Garnet	Grt[3]	*g*	
Almandine		*alm*	$Fe_3Al_2Si_3O_{12}$
Pyrope		*py*	$Mg_3Al_2Si_3O_{12}$
Grossular		*gr*	$Ca_3Al_2Si_3O_{12}$
Orthoamphibole	Oam[4]	*oa*	
Anthophyllite	Ath	*anth*	$VMg_2Mg_3(Mg_2)Si_4[Si_4]O_{22}(OH)_2$
Ferroanthophyllite		*fath*	$VFe_2Fe_3(Fe_2)Si_4[Si_4]O_{22}(OH)_2$
Gedrite	Ged	*ged*	$V\ Mg_2Mg_3\ (Al_2)Si_4[Si_2Al_2]O_{22}(OH)_2$
Hornblende	Hbl[5]	*hb*	
Tremolite		*tr*	$VCa_2Mg_3(Mg_2)Si_4[Si_4]O_{22}(OH)_2$
Ferrotremolite		*ftr*	$VCa_2Fe_3(Fe_2)Si_4[Si_4]O_{22}(OH)_2$
Tschermakite		*ts*	$VCa_2Mg_3Al_2Si_4Si_2Al_2O_{22}(OH)_2$
Pargasite		*parg*	$NaCa_2Mg_3(MgAl)Si_4[Si_2Al_2]O_{22}(OH)_2$
Plagioclase	Pl[3]		
Cl plagioclase		*C1*	
albite		*ab*	$NaAlSi_3O_8$
Fictive anorthite		*an*	$CaAl_2Si_2O_8$
Il plagioclase		*I1*	
Anorthite		*an*	$CaAl_2Si_2O_8$
Fictive albite		*ab*	$NaAlSi_3O_8$
Clinozoisite	Czo	*cz*	$Ca_2AlAl_2Si_3O_{12}(OH)$
Epidote	Ep		$Ca_2(Al,Fe^{3+})Al_2Si_3O_{12}(OH)$
Quartz	Qtz	*q*	SiO_2
Aqueous fluid	H_2O	*H_2O*	H_2O

Activity-composition relationships used in the calculations: [1] Powell *et al.* (1998); [2] Holland *et al.* (1998); [3] Vance & Holland (1993); [4] Ideal mixing on sites with $I_{ged,oa} = 24$ kJ to simulate anthophyllite-gedrite solvus; [5] Ideal mixing on sites with $I_{ts,hb} = 120–0.15T$ kJ, $I_{parg,hb} = 145–0.15T$ kJ to simulate decreasing Na and Al substitution into hornblende with decreasing temperature. See Will & Powell (1992).

limit the applicability of the results, as a wide range of amphibolite bulk compositions contain hornblende, plagioclase and quartz over a wide range of *P–T*. A potential difficulty is that, in some circumstances, a metamorphic fluid might not have been present during equilibration, or the composition of the fluid present may have been spatially or temporally variable. However, in hydrated mafic rocks being metamorphosed for the first time and without carbonate minerals, an H_2O-rich fluid phase probably would have been present, and therefore the assumption of excess aqueous vapour is probably not unduly limiting.

Representing NCFMASH as an effective ternary ($+Hbl+Pl+Qtz+H_2O$) on a triangular compatibility diagram presents various difficulties in both representation and use. Because two of the in-excess phases (hornblende and plagioclase) can vary widely in composition, finding a projection plane to make a strictly legal compatibility diagram is difficult (Powell & Sandiford, 1988) (see Worley & Powell (1998) for a solution to the analogous problem for metapelites in NCKFMASH). Moreover, because hornblende, plagioclase and quartz usually dominate the modes of amphibolites, the position of an amphibolite bulk composition projected into the compatibility diagram is very sensitive to the hornblende and plagioclase composition, and thus sensitive to *P–T*. Thus, with changing *P–T*, a specific bulk composition 'moves around' the compatibility diagram, along with the phase relationships themselves, making the diagram difficult to read in the conventional way. This problem applies equally to any projection plane in the system with $Hbl+Pl+Qtz+H_2O$ in excess. We use the AFM compatibility diagram shown in Fig. 2 with Al_2O_3, FeO, MgO at its apices. Because the projection plane does not lie between the projection phases and the projected phases, this projection is not strictly 'legal', as discussed by Powell & Sandiford (1988). However, the diagram serves to clearly illustrate the phase relationships between the aluminous phases and is only used in a semi-quantitative way. The divariant assemblages shown are projected from the calculated equilibrium hornblende and plagioclase compositions, but the sub-system equilibria and the one-phase fields are not plotted.

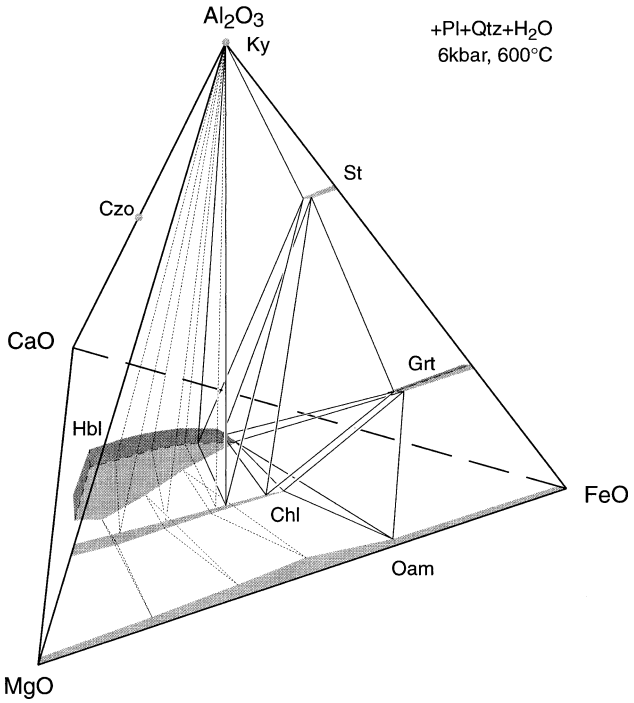

Fig. 1. Simplified CAFM (+Pl+Qtz+H_2O) compatibility diagram calculated for 600 °C and 6 kbar, with phases projected from the equilibrium plagioclase compositions. Only some of the divariant assemblages attainable for the bulk compositions dealt with in this paper are shown. Trivariant assemblages Ky–Chl–Hbl and Chl–Oam–Hbl convey the extent of the hornblende field. Plotting positions of bulk compositions are strongly influenced by the anorthite content of equilibrium plagioclase.

P–T PROJECTION FOR NCFMASH

The *P–T* projection for NCFMASH (Fig. 3) shows the univariant and invariant equilibria for all bulk compositions that have excess plagioclase + quartz + H_2O. As usual with *P–T* projections, the compositions of the phases in the univariant equilibria vary along the reaction lines, as can be seen in Table 4. The direction of increasing anorthite (X_{An}) in the plagioclase is indicated by arrows on the lines in Fig. 3. Note that many of the univariant lines emanate from CFMASH invariant points (open circles in Fig. 3).

Using the AFM (+Hbl+Pl+Qtz+H_2O) projection for this system, a series of compatibility diagrams at 6 kbar is given in Fig. 2. The series of reactions at this pressure corresponds to the classic Barrovian zones for metapelites, with orthoamphibole substituted for biotite. Also, with the same substitution, the reactions around the [Crd, Czo] invariant point at 7.9 kbar and 645 °C, correspond closely with the reactions around

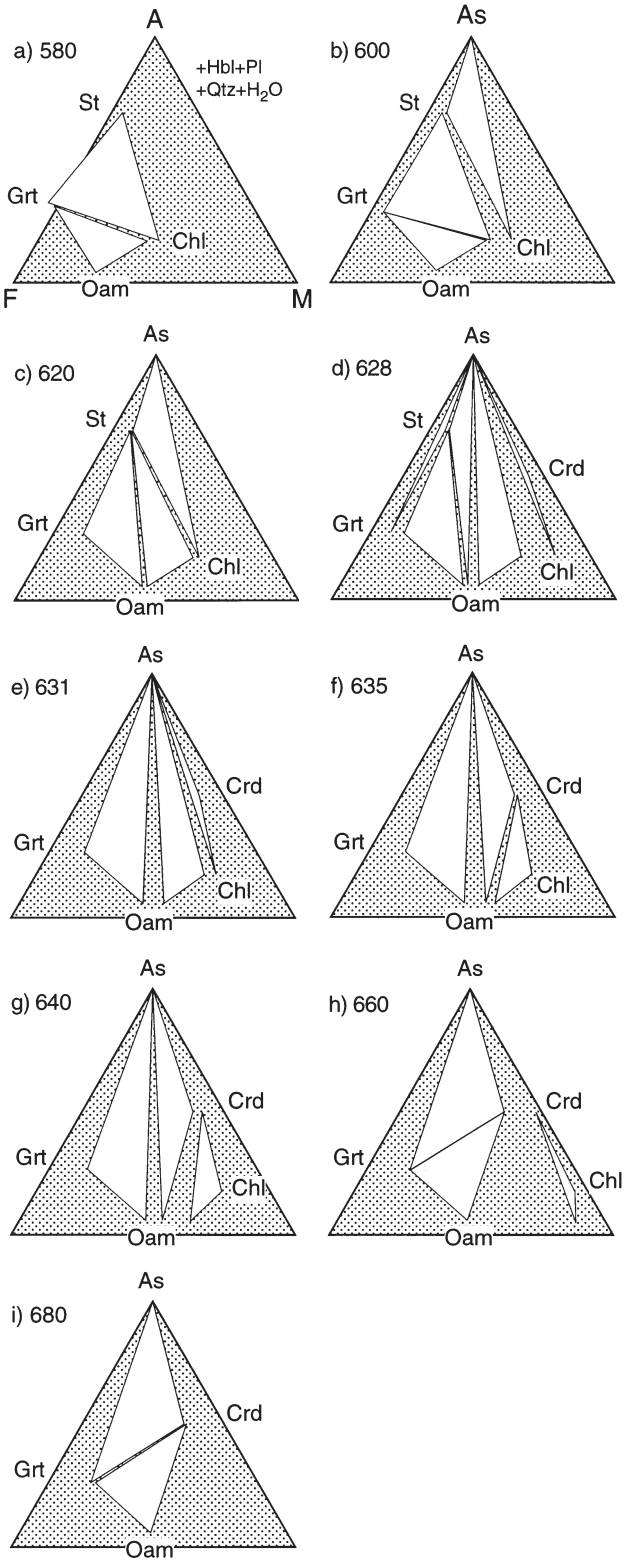

Fig. 2. A series of AFM (+Hbl+Pl+Qtz+H_2O) compatibility diagrams calculated over 580–680 °C and 6 kbar. The divariant assemblages are projected from the equilibrium hornblende and plagioclase compositions. However, the sub-system equilibria and the one-phase-fields are not plotted. Orthoamphibole (Oam) in these diagrams occupies the relative position of biotite in AFM (+Ms+Qtz+H_2O) for metapelites, and the series of reactions at this pressure corresponds to the classic Barrovian zones series of reactions for metapelites, with orthoamphibole substituted for biotite.

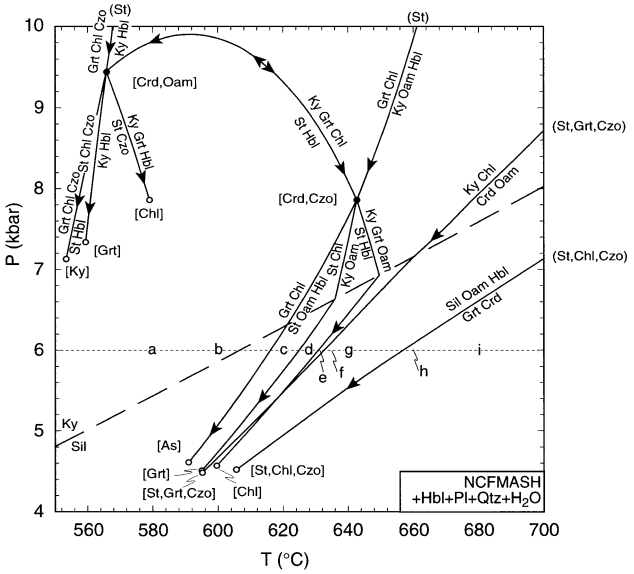

Fig. 3. *P–T* projection for the system NCFMASH with hornblende, plagioclase, quartz and H_2O in excess (hornblende is included in the labelling to help clarify reactions). For abbreviations, see Table 3. Solid circles = NCFMASH invariant points, open circles = CFMASH invariants. The direction of increasing anorthite (X_{An}) in the plagioclase is indicated by arrows on univariant lines. Invariant points and univariant lines are labelled with the absent phases in square brackets and parentheses, respectively. The univariant lines (St,Chl,Czo) and (St,Grt,Czo) are degenerate with respect to hornblende and plagioclase. The letters 'a' to 'i' along the 6 kbar line indicate the conditions of the compatibility diagrams in Fig. 2.

the metapelite AFM invariant point that closes to high pressure the staurolite + biotite field at 10 kbar and 625 °C in Powell *et al.* (1998; their Figure 3).

An additional point of interest regarding the compatibility diagrams concerns the range of hornblende and plagioclase compositions involved. Table 5 shows the compositions of the phases projected from hornblende, plagioclase, quartz and H_2O for the phase relationships at 6 kbar and 620 °C (Fig. 2c). The range of hornblende and plagioclase compositions represented is very small, even though the range of Al contents of the projected phases is very large.

PSEUDOSECTIONS FOR NCFMASH

The phase relationships depicted in Fig. 3 have little *direct* relevance to amphibolites because the majority of amphibolite assemblages have a variance greater than 2, largely due to the wide compositional ranges of the phases. Although high-variance assemblages are ultimately limited by invariant and univariant equilibria, the rocks experience only very few, if any, of the equilibria illustrated on Fig. 3. Moreover, the low-variance equilibria are very sensitive to bulk composition. Thus *P–T* projections only loosely constrain the conditions of equilibration, and, in order for phase diagrams to be really useful, they must deal directly with higher-variance assemblages.

Pseudosections provide invaluable representations of phase relationships in complex systems. They involve 'sectioning' with respect to extensive and intensive variables and show the stable mineral assemblages for a particular (fixed) bulk composition as a function of *P–T*, or over *T–X* space at constant *P*. The computer program THERMOCALC (Powell & Holland, 1988; Powell *et al.* (1998) is well suited to the construction of pseudosections because the boundaries of fields of any variance can be calculated directly (Powell *et al.*, 1998).

Phase relationships in common amphibolites

The main stable assemblages calculated for the average amphibolite A (see Table 2) are the common assemblage (the Chl–Hbl–Pl–Qtz quadrivariant) and its quinivariant sub-assemblage Hbl–Pl–Qtz (Fig. 4). At relatively low pressures orthoamphibole may occur with, or in place of, chlorite. This is consistent with the occurrence of gedrite with chlorite in the relatively low-pressure Post Pond Volcanics (Spear, 1982). The existence of aluminous and sodic clinoamphibole (here generically referred to as hornblende) at relatively high pressures is consistent with the compositional trends reported by Laird (1980).

The effect of bulk compositional change on the mineral assemblages is critical to understanding the phase relationships in high-variance rocks such as amphibolites. For example, the very restricted Ky–Hbl field ($+Pl+Qtz+H_2O$) in Fig. 4 may be expected to expand for more aluminous bulk compositions. Variation in the FeO:MgO ratio of amphibolites is also important; more Fe-rich amphibolites contain garnet in place of chlorite (e.g. Spear, 1982). Increased Na content stabilizes the Na-bearing phases plagioclase or hornblende. The following discussion details how the phase relationships of amphibolites vary with temperature and three independent compositional dimensions: the $Mg_{-1}Fe_1$ and $Ca_{-1}Al_{-1}Na_1Si_1$ exchange vectors and Al_2O_3 content. *T–X* sections describing the dependence of mineral assemblages on bulk composition are shown in Figs 5, 6 & 7.

The average amphibolite A (Table 2) is relatively magnesian, and, as a result, contains the Mg-rich mineral chlorite over a wide range of metamorphic conditions. As illustrated in Fig. 5, amphibolites at 6 kbar with X_{Fe} (FeO/FeO + MgO) in the range 0–0.54 contain chlorite ($+Hbl+Pl+Qtz+H_2O$); however, more Fe-rich rocks develop garnet-bearing assemblages (Fig. 5, $X_{Fe} > 0.54$). At higher temperatures, bulk compositional variation can be accommodated within hornblende and the quinivariant assemblage Hbl–Pl–Qtz is stable.

Variation of Na_2O : CaO ratio is achieved here via the plagioclase exchange vector ($Ca_{-1}Al_{-1}Na_1Si_1$, Fig. 6). The effect of this compositional parameter on stability fields is not immediately obvious because the substitution can be taken up entirely (according to the activity models used herein) by the excess phases,

Table 4. THERMOCALC output for the univariant assemblages around the invariant point [Crd, Czo] in Fig. 3.

P (kbar)	*T* (°C)	x(st)	x(g)	z(g)	x(oa)	y(oa)	x(hb)	y(hb)	z(hb)	an(C1)	x(chl)	y(chl)	N(chl)
Invariant													
Phases: st, g, oa, chl, ky, (hb, C1, q, fluid) or [cd,cz]													
7.9	643	0.724	0.669	0.0558	0.451	0.194	0.331	0.558	0.155	0.254	0.283	0.528	0.471
Univariant													
Phases: g + chl = st + oa (hb, C1, q, fluid) or [ky/sill]													
5.0	598	0.842	0.769	0.0848	0.627	0.198	0.493	0.533	0.0491	0.597	0.426	0.52	0.479
6.0	616	0.801	0.738	0.0719	0.56	0.198	0.428	0.546	0.0847	0.433	0.367	0.523	0.476
7.0	631	0.760	0.702	0.062	0.499	0.196	0.372	0.555	0.122	0.322	0.318	0.526	0.473
8.0	645	0.718	0.663	0.055	0.443	0.194	0.325	0.559	0.160	0.245	0.278	0.528	0.471
9.0	656	0.677	0.623	0.049	0.394	0.191	0.283	0.559	0.198	0.189	0.243	0.530	0.469
Phases: st + chl = oa + sill/ky (hb, C1, q, fluid) or [g]													
5.0	605	0.817			0.584	0.204	0.450	0.548	0.055	0.577	0.383	0.523	0.476
6.0	625	0.765			0.505	0.205	0.377	0.565	0.093	0.417	0.318	0.528	0.472
7.0	638	0.727			0.454	0.202	0.333	0.570	0.130	0.314	0.281	0.530	0.469
8.0	643	0.724			0.451	0.193	0.331	0.556	0.159	0.246	0.284	0.528	0.471
9.0	648	0.722			0.448	0.184	0.329	0.541	0.187	0.194	0.287	0.526	0.473
Phases: st = g + oa + sill/ky (hb, C1, q, fluid) or [chl]													
5.0	609	0.829	0.761	0.0774	0.607	0.204	0.475	0.558	0.0549	0.593			
6.0	631	0.783	0.723	0.0637	0.535	0.205	0.407	0.579	0.0959	0.430			
7.0	649	0.735	0.680	0.0535	0.470	0.205	0.350	0.594	0.140	0.321			
8.0	642	0.722	0.667	0.0562	0.448	0.192	0.328	0.552	0.157	0.245			
9.0	632	0.711	0.656	0.0595	0.428	0.179	0.308	0.507	0.170	0.185			
Phases: st + hb = g + chl + ky (C1, q, fluid) or [oa]													
6.0	656	0.686	0.631	0.0352			0.298	0.606	0.138	0.317	0.245	0.533	0.465
7.0	650	0.705	0.651	0.0443			0.314	0.583	0.149	0.280	0.264	0.531	0.468
8.0	641	0.728	0.672	0.0583			0.335	0.554	0.155	0.251	0.287	0.527	0.472
9.0	627	0.757	0.693	0.0831			0.363	0.518	0.154	0.231	0.319	0.524	0.475
Phases: g + chl = oa + ky (hb, C1, q, fluid) or [st]													
5.0	606		0.754	0.0755	0.591	0.213	0.457	0.566	0.050	0.611	0.390	0.525	0.474
6.0	621		0.726	0.0669	0.538	0.207	0.408	0.567	0.086	0.440	0.347	0.527	0.473
7.0	633		0.696	0.0603	0.489	0.200	0.364	0.564	0.123	0.325	0.310	0.528	0.472
8.0	644		0.664	0.0551	0.445	0.193	0.326	0.557	0.160	0.244	0.279	0.528	0.471
9.0	653		0.633	0.0511	0.404	0.186	0.292	0.548	0.197	0.187	0.252	0.528	0.471

Abbreviations: x(st) = Fe/(Fe + Mg) in staurolite; x(g) = Fe/(Fe + Mg + Ca) in garnet; z(g) = Ca/(Fe + Mg + Ca); x(oa) = Fe/(Fe + Mg) in orthoamphibole; y(oa) = Al on each of the two M2-sites; x(hb) = Fe/(Fe + Mg) in hornblende; y(hb) = Al on each of the two M2-sites; z(hb) = Na on the A-site; an(C1) = Ca/(Ca + Na) in plagioclase with C1 structure; x(chl) = Fe/(Fe + Mg) in chlorite; y(chl) = Al on M2; N(chl) is an order-disorder parameter (see Holland *et al*., 1998).

hornblende and plagioclase. In amphibolites, an increased proportion of Na_2O commonly stabilizes Na-bearing orthoamphibole; however, we find that even without an edenite molecule in the activity model for orthoamphibole, this phase is stable in more sodic amphibolites. This is in response to the relatively Al-rich and Na-poor nature of hornblende in comparison to orthoamphibole and plagioclase, respectively (e.g. Stout, 1972; Spear, 1982). Increasingly sodic bulk compositions are also decreasingly aluminous and thus stabilize sodic plagioclase and relatively Al-poor orthoamphibole (Fig. 6).

As implied by Fig. 1, Al content provides a primary control on whether aluminous minerals occur in amphibolites (Fig. 7), whereas FeO : MgO controls *which* aluminous minerals develop (see below). Figure 7 shows that, at 6 kbar, amphibolites with >24.4 mol% Al_2O_3 (as a proportion of Al_2O_3–CaO–MgO–FeO–Na_2O, see Table 2) are capable of developing aluminosilicates, cordierite and staurolite, whereas less aluminous amphibolites are composed of the minerals of the common assemblage, perhaps with the addition of orthoamphibole. The amphibolites described by Cady (1969), Cooper & Lovering (1970), Helms *et al*. (1987) and Yardley (1989) have 14.8–35.2 mol% Al_2O_3, the great majority having <24.4 mol% Al_2O_3. Thus Fig. 7 is consistent with reported amphibolite assemblages: the majority of these 'typical' amphibolites have relatively low Al contents and thus involve the minerals of the common assemblage (e.g. Laird, 1980), whereas more aluminous amphibolites contain more aluminous minerals (e.g. Selverstone *et al*., 1984). The precise composition of the transition from common amphibolites to those with aluminous minerals varies with Fe : Mg ratio, Na : Ca ratio and *P*–*T*. This explains the presence of aluminous minerals in compositionally 'typical' amphibolites with relatively low X_{Fe} and Ca contents (Helms *et al*., 1987).

Although Al content is an important influence on the occurrence of aluminous minerals, the transition from the common assemblage to aluminous assemblages is only weakly temperature-dependent. For more aluminous rocks, temperature strongly influences the nature of the specific assemblage, because many assemblages occur as sub-horizontal bands that span a wide range of Al_2O_3 contents (Fig. 7). At temperatures $<600\,^{\circ}C$, Al-rich compositions contain little or no modal hornblende, because chlorite is sufficiently mafic (and plagioclase sufficiently calcic) to accommodate the components that usually make up hornblende.

All the *P*–*T* and *T*–*X* pseudosections around bulk composition A are dominated by high-variance assemblages (Figs 4–7). None of the NCFMASH univariant reactions portrayed on the *P*–*T* projection (Fig. 3) appear on these diagrams and even divariant reactions are restricted to very narrow fields (Fig. 7). By far the

Table 5. THERMOCALC output of compatibility relationships between phases in the divariant assemblages St–Grt–Oam, St–Oam–Chl and Sil–St–Chl (+Hbl+Pl+Qtz+H_2O) for 6 kbar and 620 °C (Fig. 2c).

P (kbar)	*T* (°C)	x(st)	x(g)	z(g)	x(oa)	y(oa)	x(hb)	y(hb)	z(hb)	an(C1)	x(chl)	y(chl)	N(chl)	Projection phase	Al_2O_3	FeO	MgO	hb	C1
Phases: st, g, oa, (hb, C1, q, fluid)																			
6	620	0.7965	0.734	0.06963	0.5532	0.1999	0.4223	0.5554	0.08758	0.4321				st	0.692	0.245	0.063		
														g	0.272	0.621	0.106	0.033	−0.005
														oa	0.057	0.522	0.421		
Phases: st, oa, chl, (hb, C1, q, fluid)																			
6	620	0.7852			0.5348	0.2009	0.4043	0.5551	0.08844	0.4252	0.3441	0.5252	0.4742	st	0.692	0.242	0.066		
														oa	0.057	0.504	0.439		
														chl	0.175	0.284	0.541		
Phases : st, chl, sill, (hb, C1, q, fluid)																			
6	620	0.7669					0.3768	0.5626	0.08567	0.4425	0.3179	0.5281	0.4713	st	0.692	0.236	0.072		
														chl	0.176	0.262	0.562		
														sill	1.000				

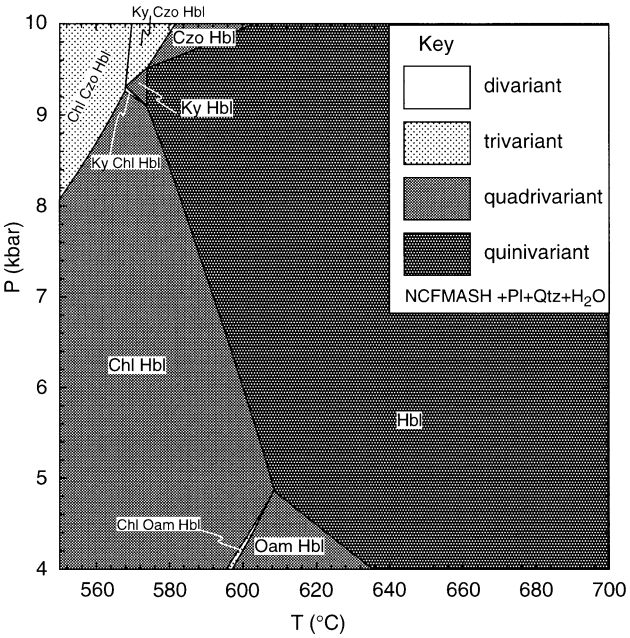

Fig. 4. *P–T* pseudosection (+Pl+Qtz+H_2O) for a typical amphibolite, bulk composition A (see Table 2). The key shows the variance of the assemblages in Figs 4–15.

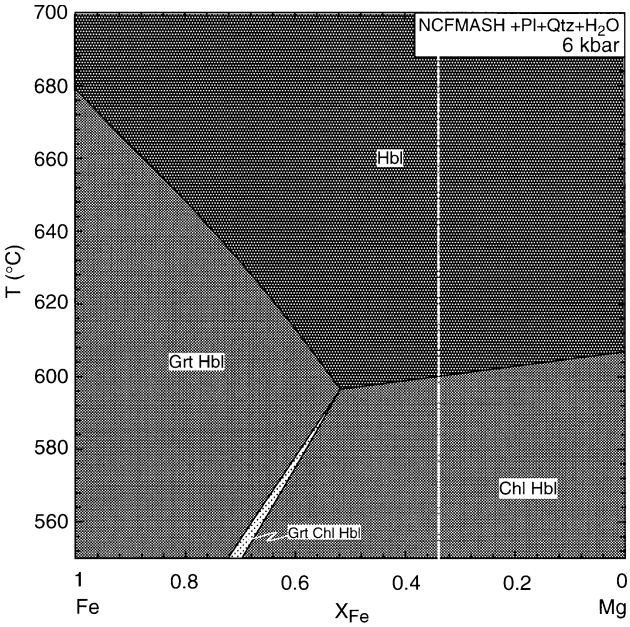

Fig. 5. T–X_{Fe} pseudosection for 6 kbar (+Pl+Qtz+H_2O) around the typical amphibolite, bulk composition A (indicated by the dot-dashed vertical line). For key see Fig. 4.

majority of amphibolites (with compositions similar to average amphibolite A) develop quinivariant, quadrivariant or trivariant assemblages as a result of metamorphism. This is in agreement with both our observations and our understanding of phase relationships in general. Indeed, it is this predominance of high-variance assemblages in nature that makes pseudosections of the total phase diagram vital and useful.

More aluminous compositions

As illustrated above, Al content is a critical control on the assemblages developed under a given set of conditions. Compositions in the range 32–35.6 mol% Al_2O_3 contain the maximum diversity of NCFMASH phases (Fig. 7), and thus yield the most information on the relationships between the assemblages. The following discussion focuses on bulk compositions with 34 mol% Al_2O_3 (composition B) that are otherwise similar to A (Table 2).

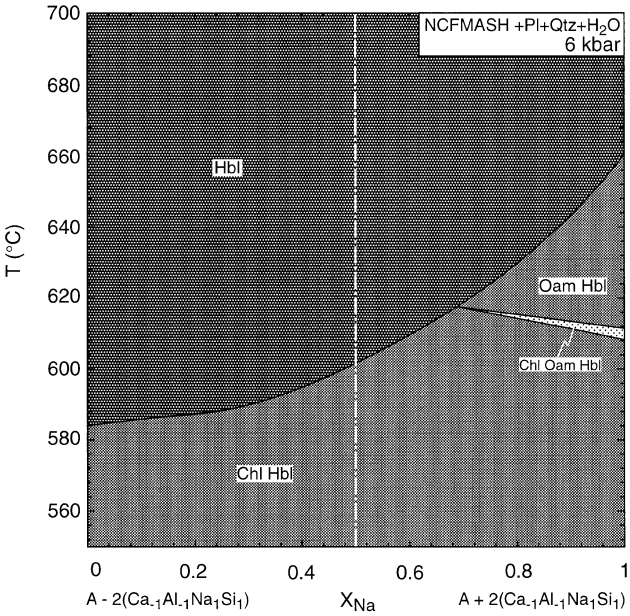

Fig. 6. T–X_{Na} pseudosection for 6 kbar (+ Pl + Qtz + H_2O) around the typical amphibolite, bulk composition A (indicated by the dot-dashed vertical line). For key see Fig. 4.

A comparison of the P–T pseudosections for the average amphibolite A (Fig. 4) and the aluminous composition B (Fig. 8) demonstrates the effect of increased Al content on the phase relationships in P–T space. The stability of kyanite-bearing assemblages is increased at the expense of the hornblende quinivariant, so that kyanite (or sillimanite) plus hornblende is stable over a wide range of pressures and temperatures. Our analysis provides quantitative support for the suggestions of Selverstone *et al.* (1984) and Ward (1984) that assemblages involving aluminous minerals such as staurolite and kyanite are stable over a more accessible region of P–T space in aluminous amphibolites compared to typical amphibolites. Orthoamphibole–hornblende-bearing amphibolites occur at higher temperatures and pressures (5.7–6.8 kbar, 625–690 °C) in more aluminous rocks. However, the assemblage chlorite–hornblende remains stable at low temperatures (Fig. 8). The As–St–Chl–Hbl, As–Chl–Hbl, AS–Chl–Oam–Hbl, As–Oam–Hbl and As–Hbl (+ Pl + Qtz + H_2O) fields all straddle the kyanite–sillimanite reaction, so that all five

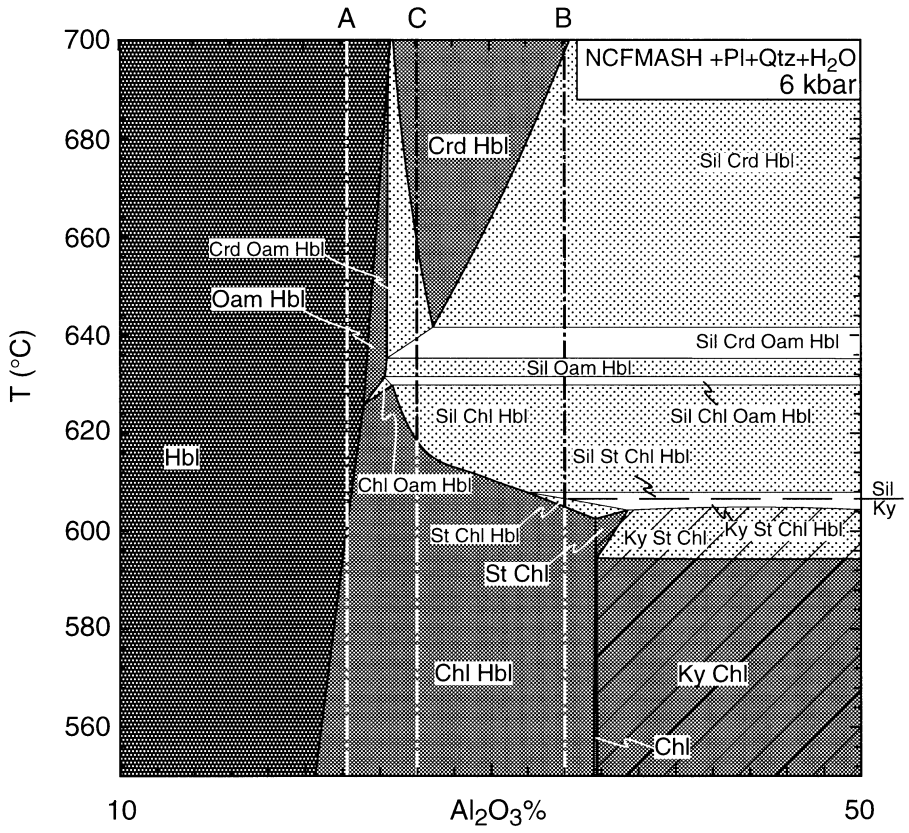

Fig. 7. T–X_{Al} pseudosection for 6 kbar (+ Pl + Qtz + H_2O) around the typical amphibolite, bulk composition A (indicated by the dot-dashed vertical line 'A'). The compositions of bulk compositions B and C (used in later figures) are shown by the dot-dashed lines labelled B and C. The hatched region in this and following diagrams indicates hornblende-absent assemblages. For key see Fig. 4.

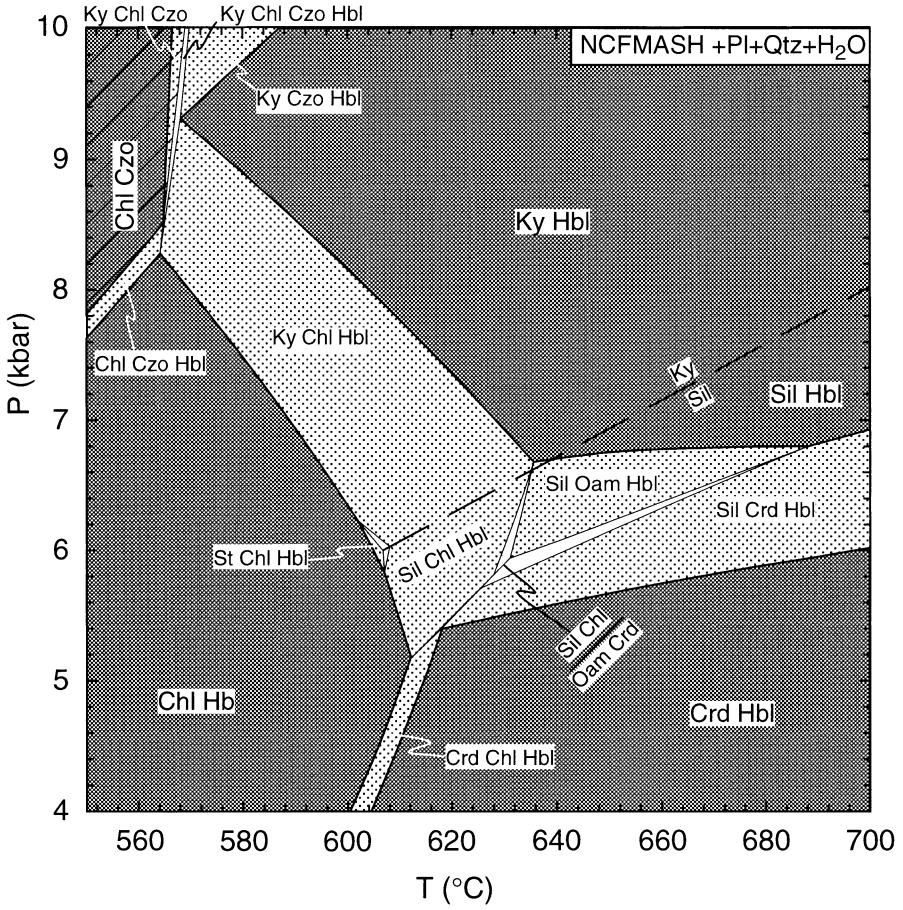

Fig. 8. *P–T* pseudosection ($+\mathrm{Pl}+\mathrm{Qtz}+\mathrm{H_2O}$) for an aluminous amphibolite, bulk composition B (see Table 2 and Fig. 7). For key see Fig. 4.

assemblages can exist with either kyanite or sillimanite. This pseudosection accounts for many of the lower-variance assemblages in amphibolites (Table 1). However, because of the magnesian nature of the bulk composition, more Fe-rich assemblages, such as those involving garnet and staurolite, either occur minimally or are not present at all in Fig. 8. In the low-T, high-P portion of Fig. 8, the proportion of hornblende decreases in response to increasing clinozoisite and plagioclase, to the extent that hornblende is unstable. The *P–T* fields in which hornblende is metastable with respect to Chl–Czo ($+\mathrm{Pl}+\mathrm{Qtz}+\mathrm{H_2O}$) are marked by hatching.

Figure 9 illustrates the effect of the plagioclase substitution on aluminous bulk compositions in the range $\mathrm{B}\pm 2\mathrm{Ca_{-1}Al_{-1}Na_1Si_1}$. This compositional change has minimal effect on mineral assemblages up to about 615 °C (at 6 kbar), because the wide ranges of possible hornblende, plagioclase and chlorite compositions allow Chl–Hbl, St–Chl–Hbl, As–St–Chl–Hbl and As–Chl–Hbl ($+\mathrm{Pl}+\mathrm{Qtz}+\mathrm{H_2O}$) to be stable over the full compositional range. In more sodic compositions, the divariant assemblages Sil–Chl–Oam–Hbl and Sil–Crd–Oam–Hbl are stable below and above the $\mathrm{Sil}+\mathrm{Chl}=\mathrm{Crd}+\mathrm{Oam}$ ($+\mathrm{Hbl}+\mathrm{Pl}+\mathrm{Qtz}+\mathrm{H_2O}$) univariant (Fig. 9). Above 650 °C, Sil–Hbl occurs in more calcic, more aluminous, less sodic rocks, whereas Sil–Crd–Hbl, Crd–Hbl and Crd–Oam–Hbl ($+\mathrm{Pl}+\mathrm{Qtz}+\mathrm{H_2O}$) occur in successively more sodic amphibolites. As discussed above, the effect of the $\mathrm{Ca_{-1}Al_{-1}Na_1Si_1}$ exchange vector on the phase relationships is dominated by its effects on hornblende and plagioclase. With increasing Na and decreasing Ca and Al, less aluminous minerals are stabilized, so that Sil–Hbl and Crd–Hbl ($+\mathrm{Pl}+\mathrm{Qtz}+\mathrm{H_2O}$) are restricted to more calcic compositions.

The FeO : MgO ratio is a critical control on mineral assemblages in hornblende-bearing rocks. As mentioned above, the phase relationships of these rocks are similar to those of metapelites (Fig. 2). This similarity appears again in Fig. 10, in which Grt–Hbl is shown as being stable in Fe-rich rocks, Chl–Hbl in Mg-rich rocks (up to 635 °C), and staurolite- and sillimanite-bearing assemblages are stable at intermediate X_{Fe} and elevated temperature (595–630 °C and >605 °C, respectively; cf. Powell *et al*., 1998; Fig. 5). In magnesian rocks, Sil–Crd–Hbl and Sil–Crd–Grt–Hbl occur at high temperatures (>620 °C). The Sil–Crd–Grt–Hbl assemblage has a biotite-bearing equivalent in metapelitic rocks, bordering the granulite facies.

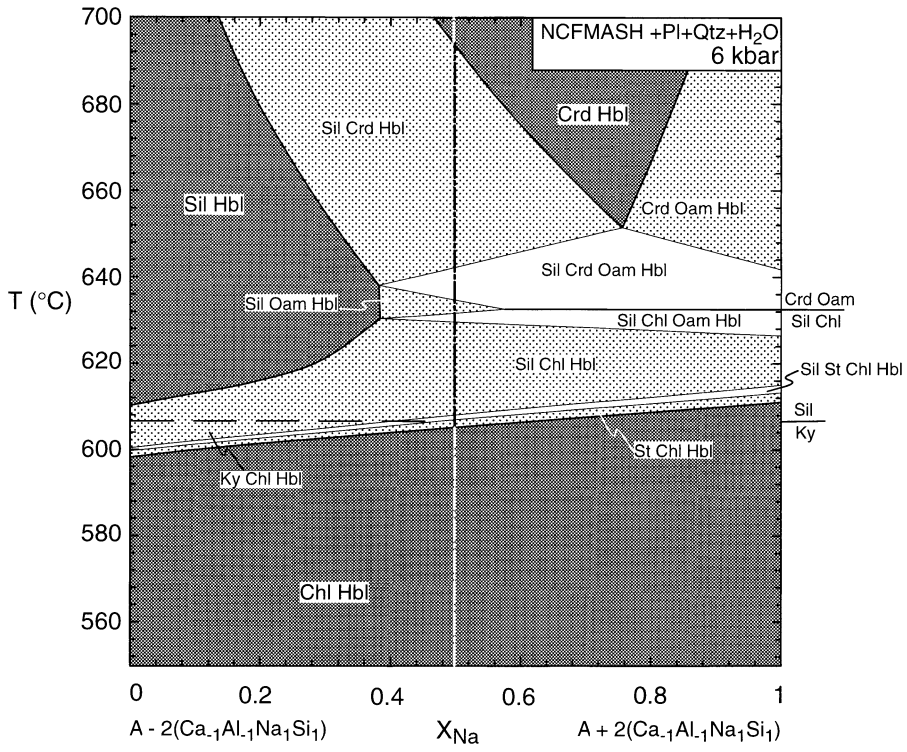

Fig. 9. T–X_{Na} pseudosection for 6 kbar ($+\mathrm{Pl}+\mathrm{Qtz}+\mathrm{H_2O}$) around the aluminous amphibolite, bulk composition B (indicated by the dot-dashed vertical line). For key see Fig. 4.

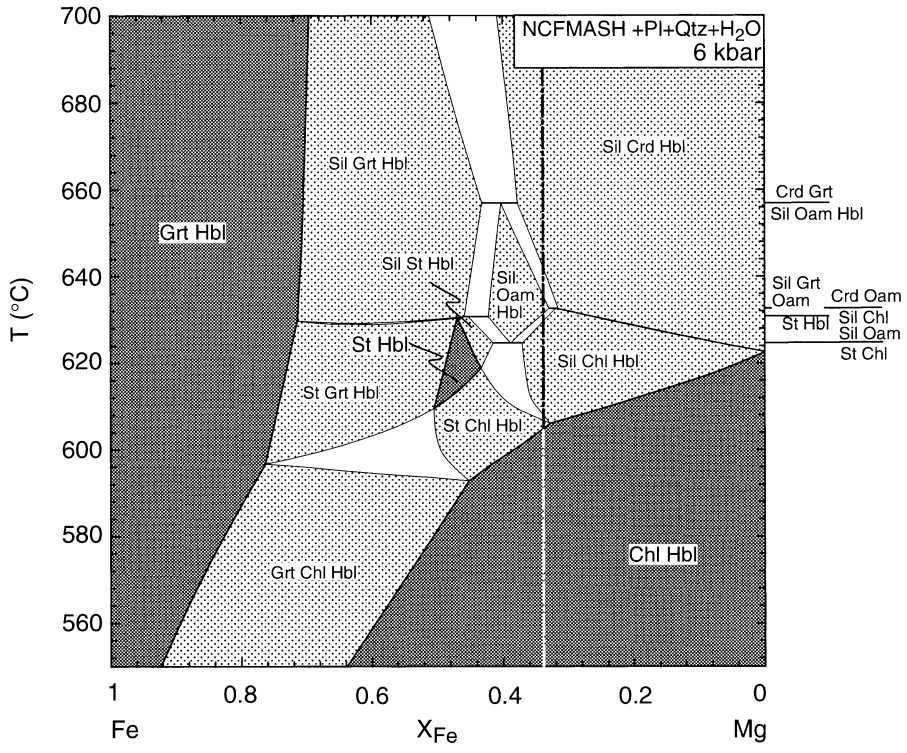

Fig. 10. T–X_{Fe} pseudosection for 6 kbar ($+\mathrm{Pl}+\mathrm{Qtz}+\mathrm{H_2O}$) around the aluminous amphibolite, bulk composition B (indicated by the dot-dashed vertical line). For key see Fig. 4.

Given that quite a number of the unusual assemblages in Table 1 involve Fe-rich phases, such as staurolite and garnet, and do not occur in Figs 4 & 8, the phase relationships in more Fe-rich compositions are worth exploring. Figure 11 illustrates the P–T dependence of phase relationships in aluminous compositions with $X_{Fe}=0.5$. In comparison to Figs 4 & 8, garnet- and staurolite-bearing assemblages are stable

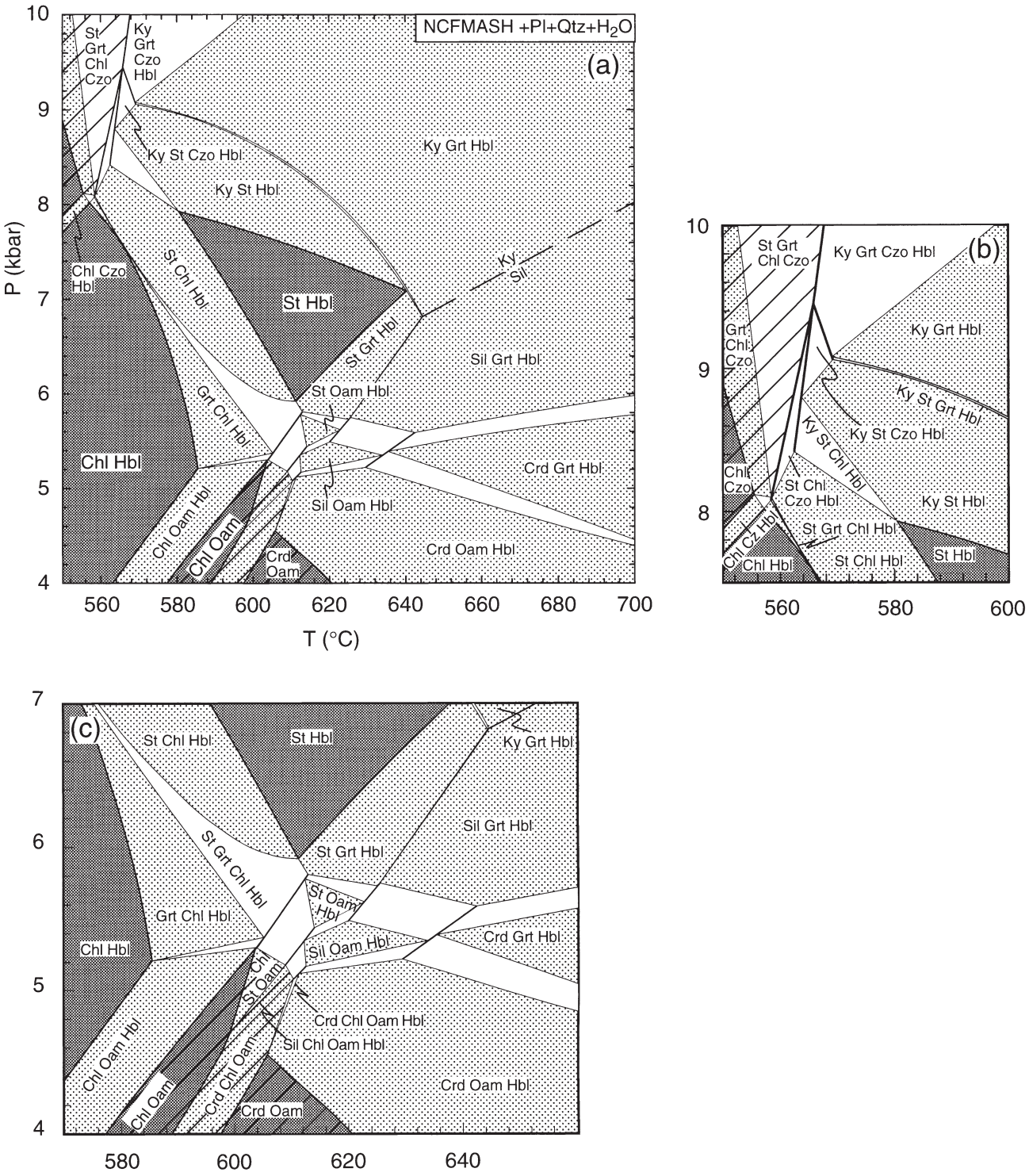

Fig. 11. *P–T* pseudosection (+Pl+Qtz+H_2O) for an aluminous but moderately Fe-rich amphibolite, based on bulk composition B (see Table 2, $X_{Fe}=0.5$ in Fig. 10). All but two of the NCFMASH univariants occur in this pseudosection. (a) Phase relationships in the region 550–700 °C and 4–10 kbar. (b) Detailed phase relationships in the region 570–660 °C and 4–7 kbar. (c) Detailed phase relationships in the region 550–600 °C and 7.5–10 kbar. For key see Fig. 4.

over a much wider *P–T* region, again in a way that mimics metapelitic rocks. Chl–Hbl is stable at low temperatures and pressures, giving way to ortho-amphibole- and then cordierite-bearing assemblages with increasing temperature. In the upper amphibolite facies, Crd–Grt–Hbl is stable. At temperatures in the range 580–620 °C, in the region marked by hatching, hornblende is metastable with respect to

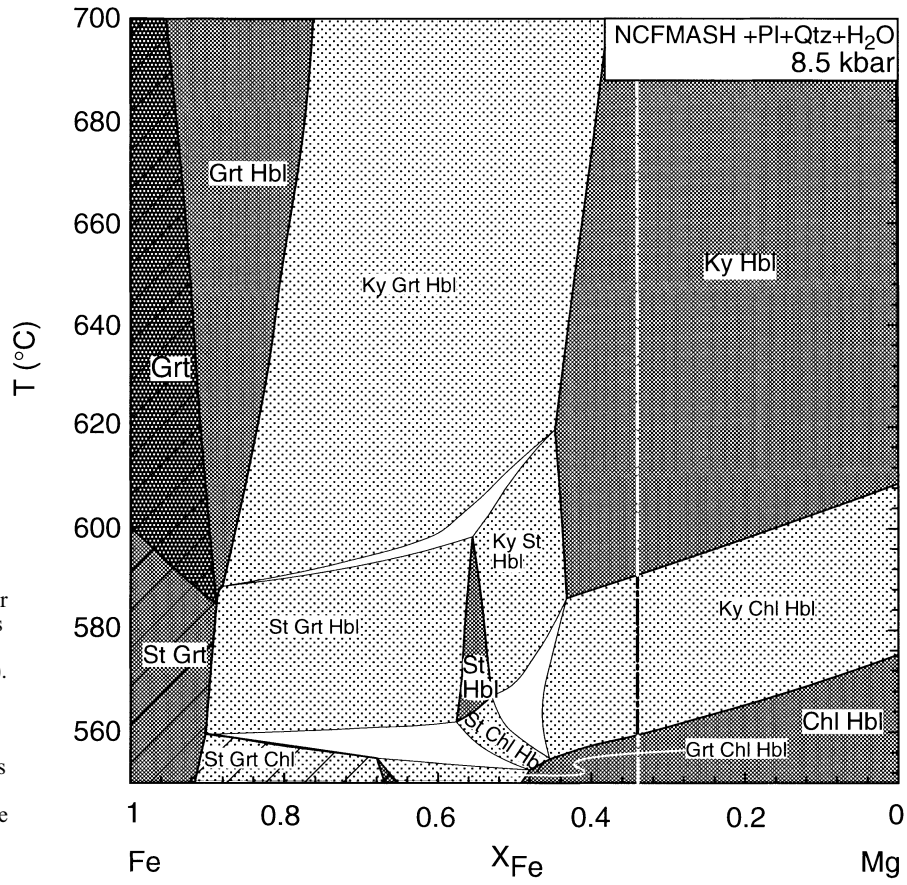

Fig. 12. T–X_{Fe} pseudosection for 8.5 kbar ($+Pl+Qtz+H_2O$) around the aluminous amphibolite, bulk composition B (indicated by the dot-dashed vertical line). Kyanite- and staurolite-bearing assemblages are stable over the majority of T–X_{Fe} space at this higher pressure (cf. Fig. 10). Clinozoisite-bearing assemblages that are stable at low temperatures have been omitted because are they obscure the relationship with Fig. 10. For key see Fig. 4.

Oam–Pl–Qtz–H_2O (Fig. 11b), whereas at high pressures and $T<570\,^{\circ}C$, hornblende is metastable with respect to Chl–Czo–Pl–Qtz–H_2O (Fig. 11c). With increasing pressure, Chl–Hbl is replaced by Grt–Hbl, and then St–Hbl and Ky–Hbl assemblages (Fig. 11). Many of the assemblages depicted in Fig. 11 have been reported in the literature (Table 1), implying that the bulk rock compositions of unusual amphibolites are commonly more Fe-rich and aluminous than the average amphibolite A. Of special note in Fig. 11 is the number of univariant assemblages that can affect rocks of this composition: all but two of the NCFMASH univariants are stable in this P–T pseudosection.

The T–X pseudosections discussed above are constructed around 6 kbar, in an attempt to represent the maximum complexity of the phase relationships. However, many kyanite and staurolite amphibolites are reported to have formed at higher pressures (e.g. Selverstone *et al.*, 1984; Ward, 1984; Grew & Sandiford, 1985; Helms *et al.*, 1987). Although the relationships between the higher-pressure assemblages are broadly similar to their low-pressure counterparts, there are important differences (compare Fig. 12 at 8.5 kbar and Fig. 10). Most obvious are the greatly increased stability fields of Ky–Hbl and the lack of both cordierite and orthoamphibole at higher pressures. This is consistent with observations from the literature: Schumacher & Robinson (1987), Humphreys (1993) and Arnold *et al.* (1995) reported cordierite with hornblende and generally an orthoamphibole. In all three occurrences, the estimated pressures are less than about 7 kbar.

The most reactive temperature window at lower pressure encompasses continuous and discontinuous reactions involving sillimanite, staurolite, cordierite, garnet, chlorite, orthoamphibole and hornblende ($+Pl+Qtz+H_2O$), between 600 and 650 °C (Fig. 10). At 8.5 kbar, this window occurs at lower temperatures, around 550–620 °C (Fig. 12) and involves kyanite, staurolite, garnet, chlorite and hornblende. For very Fe-rich compositions, the proportion of hornblende decreases to zero as the grossular content of garnet increases past about $X_{grs}=0.2$, and a number of quadrivariant and quinivariant hornblende-absent fields result (shown by hatching in Fig. 12). Some of the assemblages in the low-temperature part of Fig. 12 are metastable with respect to clinozoisite-bearing assemblages, which are omitted because they obscure the relationship between Figs 10 and 12.

Moderately aluminous amphibolites

The very aluminous bulk compositions dealt with above are able to develop aluminosilicate-, staurolite- or cordierite-bearing assemblages over a wide range of

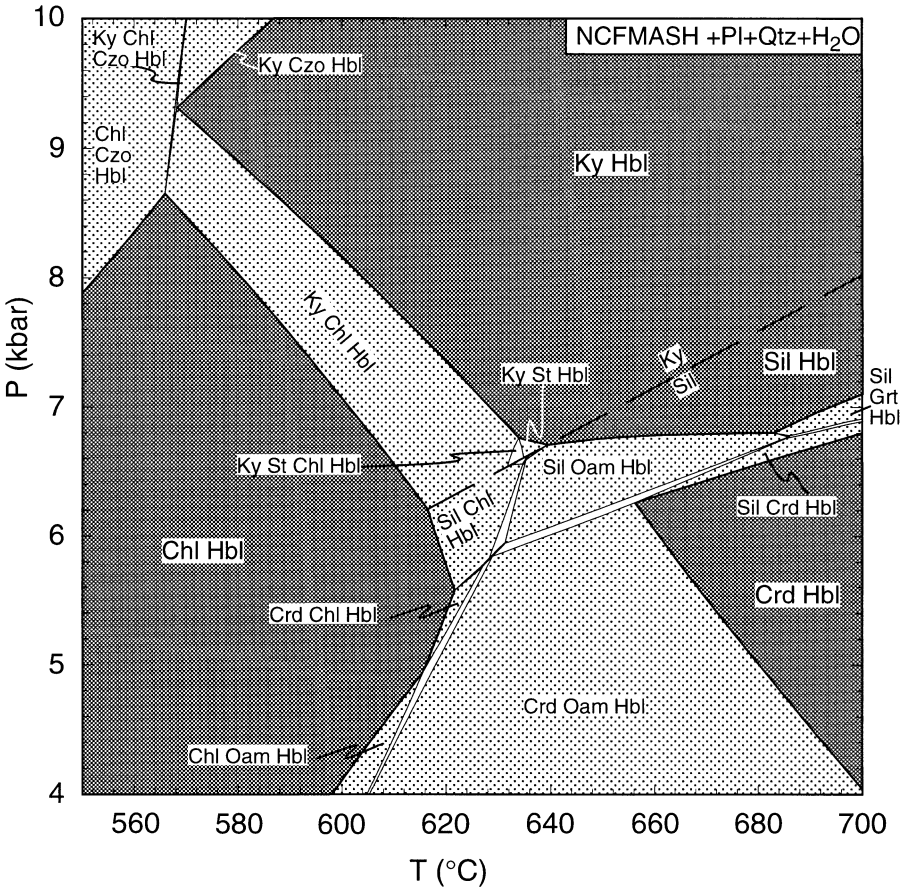

Fig. 13. *P–T* pseudosection ($+\mathrm{Pl}+\mathrm{Qtz}+\mathrm{H_2O}$) for a moderately aluminous amphibolite, bulk composition C (see Table 2 & Fig. 7). For key see Fig. 4.

P–T conditions (Figs 8 & 11). However, although these types of assemblages have been reported from geographically widespread localities of a variety of ages and settings, the number of occurrences is relatively small. As outlined above, this suggests that either the conditions required for the formation of aluminous assemblages are rarely attained, or that the compositions of the rocks involved are unusual. An intermediate position is probably more realistic: staurolite and kyanite amphibolites are rare because the appropriate stability fields occupy only relatively small regions of *P–T and* compositional space. If so, the *P–T* and *T–X* pseudosections constructed for very aluminous amphibolites give an exaggerated impression of the region over which St–Hbl, As–Hbl and related assemblages are stable. Figures 13–15 for bulk composition C (26 mol% Al_2O_3, see Fig. 7 and Table 2) present a somewhat more realistic picture, in which the amphibolites are sufficiently aluminous to stabilize aluminous phases, but are not so extreme that aluminous assemblages occur over a wide *P–T–X* area. The phase relationships for the moderately aluminous amphibolite C (Fig. 13) are similar to (though more restricted than) those of the more aluminous composition, B (34 mol% Al_2O_3, Figs 8 & 10). Composition C is within the range of analyses presented by Cady (1969), Cooper & Lovering (1970), Helms *et al.* (1987) and Yardley (1989), and so can be viewed as a fairly typical amphibolite.

For relatively low-temperature amphibolites, chlorite-, kyanite- and clinozoisite-bearing assemblages are predicted to be stable, as is generally observed in upper greenschist and blueschist facies metabasites (e.g. Laird, 1980; Fig. 13). High-pressure amphibolites develop kyanite (or kyanite–garnet in Fe-rich rocks, Fig. 15) over a wide range of temperatures, whereas cordierite (or orthoamphibole or garnet–orthoamphibole in Fe-rich compositions) is stable in high-*T*, low-*P* amphibolites (Figs 14 & 15). Kyanite–staurolite amphibolites may develop in Fe-rich compositions (Fig. 15), but this assemblage is restricted to a very small *P–T* window in more magnesian rocks (Fig. 13). Many of the assemblages listed in Table 1 are stable for this moderately aluminous model bulk composition.

TESTING THE CALCULATED PHASE RELATIONSHIPS

Although the assemblages of interest in this paper are by no means common, they have been recorded from more than 14 different geographically and geologically diverse locations. The majority of workers have been content to document the existence of staurolite- or kyanite-bearing amphibolites and to interpret them as

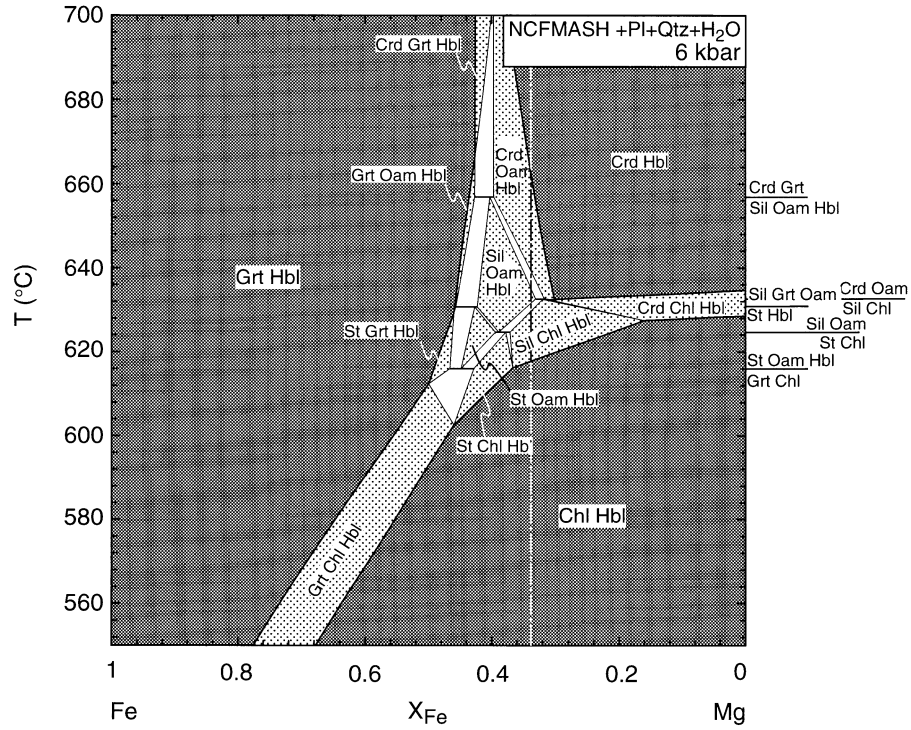

Fig. 14. T–X_{Fe} pseudosection for 6 kbar ($+\mathrm{Pl}+\mathrm{Qtz}+\mathrm{H_2O}$) around the moderately aluminous amphibolite, bulk composition C (indicated by the dot-dashed vertical line). These phase relationships are quite similar to those for the more aluminous amphibolite (Fig. 10). However, the compositional range over which sillimanite and staurolite-bearing assemblages are stable is much narrower in this more moderately aluminous composition. For key see Fig. 4.

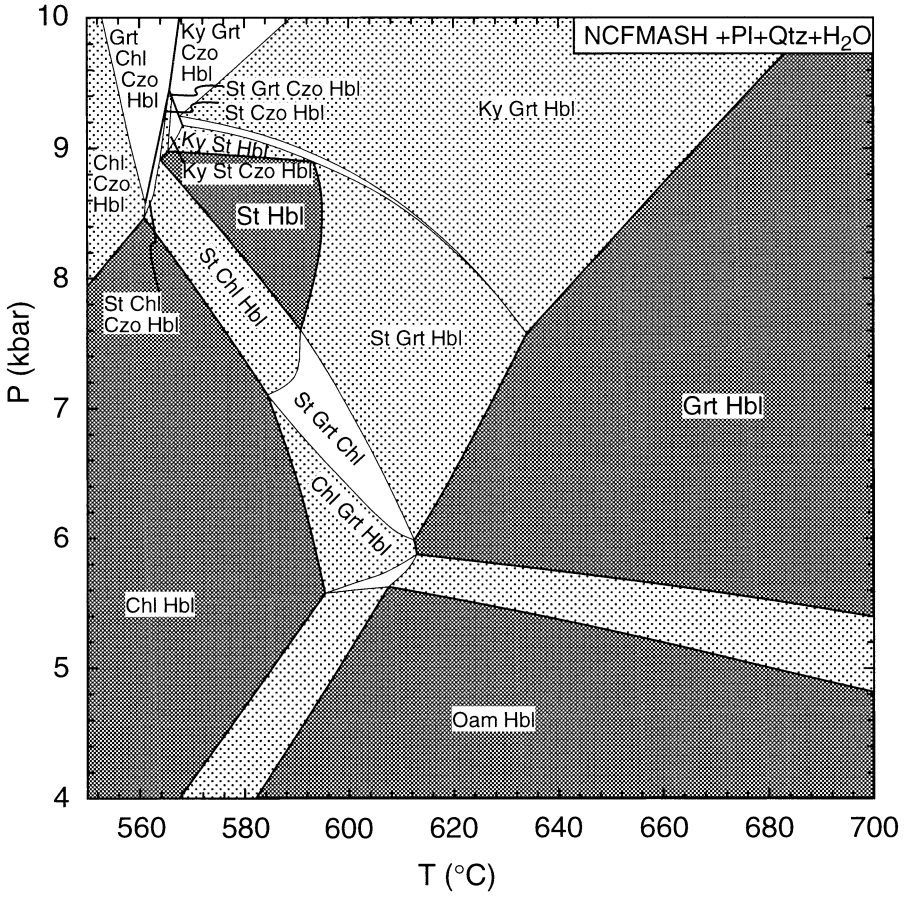

Fig. 15. P–T pseudosection ($+\mathrm{Pl}+\mathrm{Qtz}+\mathrm{H_2O}$) for a moderately aluminous and moderately Fe-rich amphibolite based on bulk composition C (see Table 2, $X_{Fe}=0.5$ in Fig. 14). Only the clinozoisite-bearing univariant reactions occur in this phase diagram (cf. Fig. 11). For key see Fig. 4.

evidence of high-pressure metamorphism, based on the work of Selverstone *et al.* (1984). Table 1 lists these assemblages, using the nomenclature of the phase diagrams presented here and arranged for ease of comparison with the calculated grid. It provides a good indication of not only what assemblages have been reported, but also what lower-variance fields, lines and points should consequently be stable in the grid. Table 1 indicates that there is strong evidence in the literature to support the stable existence of a number of univariant equilibria. Direct evidence for six of these—(Crd, Grt, Oam), (Crd, Chl, Oam), (As, Crd, Oam), (Crd, Grt, Czo), (As, Crd, Czo) and (Grt, Chl, Czo)—exists in rocks. The stability of an additional five univariants is inferred by the combination of higher-variance assemblages—(Crd, Oam, Czo), (St, Crd, Oam), (Crd, Chl, Czo), (St, Grt, Czo) and (St, Chl, Czo)—as shown in Table 1. All these occur in the phase diagrams discussed here, with the exception of the univariant (Grt, Chl, Czo). The absence of this univariant assemblage in the calculated grid is discussed below.

The assemblage Ky–St–Grt–Chl–Ep–Hbl–Pl–Qtz has been reported by Selverstone *et al.* (1984). The stability of this NCFMASH invariant assemblage [Crd, Oam] is consistent with the other reported assemblages, and the calculated invariant point occurs at 565 °C and 9.5 kbar (Fig. 3). These conditions are a little higher in pressure than the *c.* 550 °C and 6–8 kbar estimated for the down-pressure segment of the *P–T* path of Selverstone *et al.* (1984). This is consistent with the stabilization of garnet by Mn, as suggested by Selverstone *et al.* (1984). The univariant assemblages listed above also imply the stable existence of the NCFMASH invariant assemblage [Crd, Czo] (and perhaps [Chl, Czo], see below). Thus, the NCFMASH grid should contain at least the two invariants [Crd, Oam] and [Crd, Czo], linked by univariant assemblages, most of which are reported in nature. Of the reported univariants, only (St, Chl, Czo), (St, Grt, Czo) remain unlinked to the main grid. Not all univariants in a phase diagram need to intersect in full-system invariant points, and (St, Chl, Czo) and (St, Grt, Czo) simply exist between the sub-system CFMASH and NFMASH invariant points, without intersecting any other NCFMASH univariants (Fig. 3; however, see below).

The occurrence of the univariant assemblage Sil–St–Crd–Ged–Hbl (Grt, Chl, Czo) in New Hampshire (Schumacher & Robinson, 1987) and its sub-assemblages St–Crd–Ged–Hbl and Sil–St–Crd–Hbl (+Pl+Qtz) in South Africa (Humphreys, 1993), despite their metastability in Fig. 3, may be due to several factors. One or more of the minerals may be stabilized outside its NCFMASH stability field by the presence of additional components (e.g. Zn in staurolite). Reduced water activity (a_{H_2O}) or uncertainties in the thermodynamic data or activity–composition (*a–X*) relationships also may cause relative movement of the univariants in Fig. 3 to stabilize the missing assemblages. Figure 16(a) illustrates the effects of additional Zn, reduced a_{H_2O} and increased non-ideality of gedrite in orthoamphibole on the positions of the NCFMASH univariants (St, Chl, Czo) and (Crd, Chl, Czo). Additional Zn is crudely modelled by reducing the activity of the *fst* and *mst* end-members, whereas increasingly non-ideal orthoamphibole is achieved by increasing the I-value of gedrite in the Darken quadratic formalism (DQF) term for orthoamphibole (Will & Powell, 1992). The intersection of these two univariants would stabilize the sub-assemblages of [Chl, Czo] that are reported by Schumacher & Robinson (1987) and Humphreys (1993), but are not stable in Fig. 3. Calculations show that both incorporation of Zn into staurolite and non-ideality in orthoamphibole are capable of stabilizing the new invariant point [Chl, Czo]. Reduced a_{H_2O} would lower the *P* and *T* of the reactions (St, Chl, Czo) and (Crd, Chl, Czo), respectively, making a stable intersection less likely (Fig. 16a).

Both the South African and New Hampshire assemblages contain Zn-bearing staurolites with up to 3.47 wt% ZnO or 0.7 Zn per formula unit, based on 46 oxygens (Schumacher & Robinson, 1987) and up to 0.51 wt% or 0.1 Zn per formula unit (Humphreys, 1993), respectively. However, these values are considerably less than the 1.8 Zn per formula unit ($a_{znst} = 0.04$) required for the intersection of (Crd, Chl, Czo) and (St, Chl, Czo). Bearing in mind the simple *a–X* model adopted for orthoamphibole here and the absence of the edenite end-member from the model, the DQF term for gedrite could have been under-estimated by around 6 kJ/mol, so that the topology shown in Fig. 16(b) is reasonable.

The most satisfactory explanation for the occurrence of Sil–St–Crd–Oam–Hbl–Pl–Qtz (Grt, Chl, Czo) and sub-assemblages in nature is a combination of the effects of minor components, together with uncertainty in thermodynamic data and *a–X* relationships. That the invariant [Chl, Czo] should be stable (or almost stable in the model system) in at least some instances is consistent with the observation in nature of the univariant (Grt, Chl, Czo) and the St–Crd assemblages reported by a number of workers. Its stability is also supported by the observation of St–Crd in Ca-poor amphibolites and K-poor metapelites that approximate the FMASH system, namely cordierite–orthoamphibole-type rocks (e.g., Robinson & Jaffe, 1969; Helms *et al.*, 1987; Schumacher & Robinson, 1987; Arnold & Sandiford, 1990).

In summary, the calculated phase relationships presented here are largely consistent with the majority of observed mineral assemblages, including approximate mineral compositions and equilibration conditions (Table 1). Some difficulty remains over the stability of sillimanite or kyanite in amphibolites. However, together with the uncertainty in the location of the kyanite–sillimanite transition and the

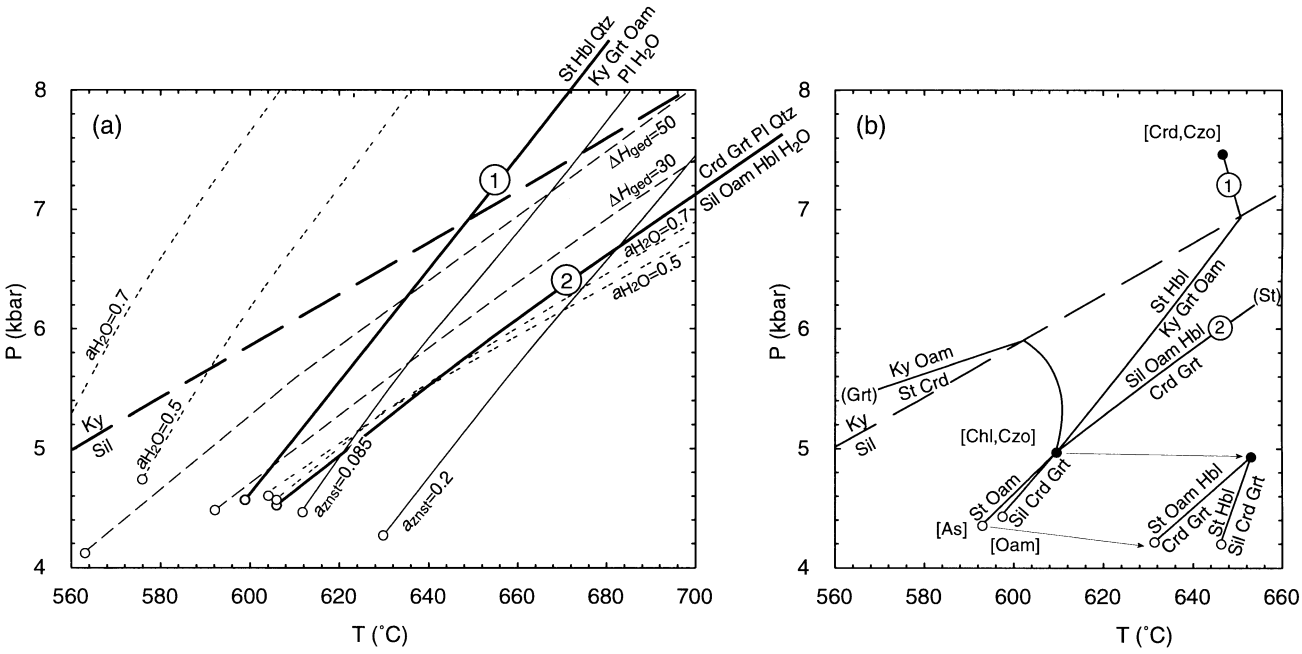

Fig. 16. *P–T* diagrams illustrating the effect of Zn in staurolite, reduced a_{H_2O} and more non-ideal orthoamphibole on the positions of the NCFMASH univariants 1 (Crd, Chl, Czo) and 2 (St, Chl, Czo) originally shown in Fig. 3. (a) *P–T* diagram showing that intersection of the two univariants (bold solid lines) could be achieved with a Zn content such that $a_{znst} < 0.085$ (narrow solid lines), or a more non-ideal orthoamphibole, e.g. $\Delta H_{ged} = 30$ (short dashed lines). Reduced a_{H_2O} would lower the *T* and *P* of the reactions (Crd, Chl, Czo) and (St, Chl, Czo), respectively, making a stable intersection unlikely (dotted lines). The kyanite–sillimanite boundary (bold dashed lines) is shown for reference; however, for clarity, all equilibria are calculated with sillimanite. Thus the higher pressure univariants are metastable with respect to kyanite. (b) *P–T* diagram ($+\mathrm{Hbl}+\mathrm{Pl}+\mathrm{Qtz}+\mathrm{H_2O}$) showing the topology of univariant curves around the invariant point [Chl, Czo], calculated with $\Delta H_{ged} = 30$. To aid in visualization, Hbl is included in the labels.

NCFMASH reactions themselves, the often-observed metastable persistence of aluminosilicates in experimental and natural rocks suggests that this is not a major deficiency in the calculated grid. The level of consistency achieved implies that the *P–T* projection is a valid representation of the phase relationships in staurolite and kyanite amphibolites, and the *P–T*, and *T–X* pseudosections derived from it are also sound.

DISCUSSION

The phase relationships presented here emphasize the importance of bulk composition, as well as physical environment (pressure and temperature), on the formation of mineral assemblages in amphibolites. The Al content of amphibolites is critical in determining whether assemblages such as kyanite–hornblende and staurolite–hornblende can develop in place of the common assemblage of Laird (1980). In amphibolites that exceed the Al threshold, the ratio of Fe to Mg, and to a lesser extent Na to Ca, determines the precise nature of the aluminous assemblages. As in metapelitic rocks, Fe-rich amphibolites tend to contain garnet and staurolite, whereas more magnesian rocks contain chlorite or cordierite. Aluminous amphibolites with intermediate X_{Fe} generally contain aluminosilicates or orthoamphibole or combinations of Fe- and Mg-rich minerals, depending on their equilibration conditions and proportion of Al_2O_3.

The calculated stability fields for staurolite- and kyanite-bearing amphibolites occur at pressures > 5.5 kbar, providing quantitative support for the restriction of these assemblages to elevated pressures (Selverstone *et al.*, 1984). However, continuous reactions, rather than the discontinuous reactions suggested by Selverstone *et al.* (1984), are vital in forming these assemblages. The phase diagrams presented herein suggest that there is far more information to be gained from these assemblages than has been considered in the past. The strong influence of Al content and X_{Fe} on the *P–T* distribution of assemblages means that these types of rocks have a greater potential for constraining *P–T* evolution than has generally been recognized (e.g. Helms *et al.*, 1987; Whitney, 1992). Quite small variations in bulk composition can cause changes in the assemblages, and potentially, the range of reaction textures relating them. In combination, such occurrences might constrain near-complete *P–T* paths (e.g. Arnold *et al.*, 1995) and so help us to better understand the terranes in which they occur.

ACKNOWLEDGEMENTS

We thank F.S. Spear, J. Selverstone and D. Ellis for helpful reviews, and R. H. Vernon for a thorough editorial job. J.A. thanks the Department of Geosciences at the University of Massachusetts, Amherst, for hospitality while revisions were carried out.

REFERENCES

Arnold, J., 1994. Staurolite–kyanite-amphibolites: Calculated phase relations with application to amphibolites from the Harts Range, central Australia and the Zillertaler Alpen, Austria. *Unpublished PhD Thesis, University of Adelaide, South Australia.*

Arnold, J. & Sandiford, M., 1990. Petrogenesis of cordierite–orthoamphibole assemblages from the Springton region, South Australia. *Contributions to Mineralogy and Petrology*, **106,** 100–109.

Arnold, J., Sandiford, M. & Wetherley, S., 1995. Metamorphic events in the eastern Arunta Inlier: Part 1. Metamorphic petrology. *Precambrian Research*, **71,** 183–205.

Cady, W. M., 1969. Regional tectonic synthesis of northwestern New England and adjacent Quebec. *Geological Society of America Memoir*, **120**.

Cooper, A. F. & Lovering, J. F., 1970. Greenschist amphiboles from the Haast River, New Zealand. *Contributions to Mineralogy and Petrology*, **27,** 11–24.

Frey, M., Trommsdorff, V. & Wenk, E., 1980. Alpine metamorphism of the Central Alps. In: *Geology of Switzerland. A Guide Book. Part B: Geological Excursions* (eds Trümpy, R., Homewood, P. W., Ayrton, S., Fischer, H. and Schweizerische Geologische Kommission), pp. 295–316. Wepf & Co., Basel.

Gibson, G. M., 1978. Staurolite in amphibolite from the Upper Seaforth River, central Fiordland, New Zealand. *Mineralogical Magazine*, **42,** 153–154.

Grew, E. S. & Sandiford, M., 1985. Staurolite in a garnet–hornblende–biotite schist from the Lanterman Range, northern Victoria Land, Antarctica. *Neues Jahrbuch für Mineralogie: Monatschefte*, **9,** 396–410.

Helms, T. S., McSween, H. Y., Labotka, T. C. & Jarosewich, E., 1987. Petrology of a Georgia Blue Ridge amphibolite unit with hornblende + gedrite + kyanite + staurolite. *American Mineralogist*, **72,** 1086–1096.

Holland, T. J. B. & Powell, R., 1990. An enlarged and updated internally consistent thermodynamic dataset with uncertainties and correlations: the system K_2O–Na_2O–CaO–MgO–MnO–FeO–Fe_2O_3–Al_2O_3–TiO_2–SiO_2–C–H_2–O_2. *Journal of Metamorphic Geology*, **8,** 89–124.

Holland, T. J. B., Baker, J. & Powell, R., 1998. Mixing properties and activity–composition relationships of chlorites in the system MgO–FeO–Al_2O_3–SiO_2–H_2O. *European Journal of Mineralogy*, **10,** 395–406.

Humphreys, H. C., 1993. Metamorphic evolution of amphibole-bearing aluminous gneisses from the Eastern Namaqua Province, South Africa. *American Mineralogist*, **78,** 1041–1055.

Laird, J., 1980. Phase equilibria in mafic schist from Vermont. *Journal of Petrology*, **21,** 1–37.

Mahar, E., Baker, J., Powell, R. & Holland, T. J. B., 1997. The effect of Mn on mineral stability in pelites. *Journal of Metamorphic Geology*, **15,** 223–238.

Powell, R. & Holland, T. J. B., 1988. An internally consistent thermodynamic dataset with uncertainties and correlations: 3: application methods, worked examples and a computer program. *Journal of Metamorphic Geology*, **6,** 173–204.

Powell, R. & Sandiford, M., 1988. Sapphirine and spinel phase relationships in the system FeO–MgO–Al_2O_3–SiO_2–TiO_2–O_2 in the presence of quartz and hypersthene. *Contributions to Mineralogy and Petrology*, **98,** 64–71.

Powell, R., Holland, T. J. B. & Worley, B., 1998. Calculating phase diagrams involving solid solutions via non-linear equations, with examples using THERMOCALC. *Journal of Metamorphic Geology*, **16,** 577–588.

Purtscheller, F. & Mogessie, A., 1984. Staurolite in garnet amphibolite from Sölden, Ötztal old crystalline basement, Austria. *Tschermaks Mineralogische und Petrographische Mitteilungen*, **32,** 223–233.

Robinson, P. & Jaffe, H. W., 1969. Chemographic exploration of amphibole assemblages from central Massachusetts and southwestern New Hampshire. *Mineralogical Society of America, Special Paper*, **2,** 251–274.

Schumacher, J. C. & Robinson, P., 1987. Mineral chemistry and metasomatic growth of aluminous enclaves in gedrite–cordierite gneiss from southwestern New Hampshire. *Journal of Petrology*, **28,** 1033–1073.

Selverstone, J., Spear, F. S., Franz, G. & Morteani, G., 1984. High pressure metamorphism in the SW Tauern Window, Austria: *P–T* paths from hornblende–kyanite–staurolite schists. *Journal of Petrology*, **25,** 501–531.

Spear, F. S., 1982. Phase equilibria of amphibolites from the Post Pond Volcanics, Mt Cube Quadrangle, Vermont. *Journal of Petrology*, **23,** 383–426.

Spear, F. S. & Rumble, D., 1986. Pressure, temperature, and structural evolution of the Orfordville Belt, west-central New Hampshire. *Journal of Petrology*, **27,** 1071–1093.

Stout, J., 1972. Phase petrology and mineral chemistry of coexisting amphiboles from Telemark, Norway. *Journal of Petrology*, **13,** 99–145.

Thompson, J. B., 1957. The graphical analysis of mineral assemblages in pelitic schists. *American Mineralogist*, **42,** 842–858.

Vance, D. & Holland, T. J. B., 1993. A detailed isotopic and petrological study of a single garnet from the Gassetts Schist, Vermont. *Contributions to Mineralogy and Petrology*, **114,** 101–118.

Ward, C. M., 1984. Magnesium staurolite and green chromian staurolite from Fiordland, New Zealand. *American Mineralogist*, **69,** 531–540.

Whitney, D. L., 1992. High-pressure metamorphism in the Western Cordillera of North America: an example from the Skagit Gneiss, North Cascades. *Journal of Metamorphic Geology*, **10,** 71–85.

Will, T. M. & Powell, R., 1992. Activity–composition relationships in multi-component amphiboles: an application of DQF. *American Mineralogist*, **77,** 954–966.

Worley, B. & Powell, R., 1998. Singularities in NCKFMASH (Na_2O–CaO–K_2O–MgO–FeO–Al_2O_3–SiO_2–H_2O). *Journal of Metamorphic Geology*, **16,** 169–188.

Yardley, B. W. D., 1989. *An Introduction to Metamorphic Petrology*. Longman Group UK Ltd, Harlow, Essex.

Received 31 August 1998; revision accepted 10 July 1999.